41st IEEE Industrial Electronics Society Conference (IECON), Yokohama (Japan), Nov. 2015

DOI: 10.1109/IECON.2015.7392204

Synchronous Reluctance Motor Multi-Static MEC Model

G. Bueno Mariani
A. Besri
N. Voyer
C. Chillet
M. Fassenet
L. Garbuio

Synchronous Reluctance Motor Multi-Static MEC Model

G. Bueno Mariani, A. Besri, N. Voyer
Mitsubishi Electric R&D Centre Europe
1, allée de Beaulieu
CS 10806
35708 RENNES CEDEX 7

C. Chillet, M. Fassenet, L. Garbuio
Univ. Grenoble Alpes, G2Elab, F-38000 Grenoble, France
CNRS, G2Elab, F-38000Grenoble, France

***Abstract*—High efficiency, low cost and high reliability electrical machines are designed to meet very demanding specifications for a wide range of applications. The SynchRM (Synchronous Reluctance Motor) has very interesting properties and features. One of the main advantages is that the motor can be designed without rare earth materials permanent magnets. In this article, a modeling method of such machines using the MEC (Magnetic Equivalent Circuit) is proposed. The main challenges are to obtain a very accurate model in order to calculate torque variations and be a parametric model for optimization. For this a precise air gap modeling is needed. For future work this model is going to be first coupled with an electrical circuit for control design and secondly used for machine optimization.**

Keywords—Synchronous Reluctance Motor (SyncRM), Magnetic Equivalent Circuit (MEC), Reluctance Network, Motor modeling, Air gap modeling.

I. INTRODUCTION

Motor modeling was widely studied over the years, some methods are well known for low computational cost, while others for accuracy. On the domain of modeling electromagnetic motors the 2-D FEM (Finite Element Method) is a well know method, which results are close to the reality. However it is costly in terms of computational time. On the other hand, analytical models exhibit low computational cost, but are not very accurate when the studied geometries become complex. The intermediary solution can be the MEC (Magnetic Equivalent Circuit), which is also known as Semi-Analytical model. MEC presents a good compromise between computational cost and accuracy [1].The model is built on the environment of [18]. This environment allows accessing the Jacobean of the output parameters, which can be used to motor optimization and also to access the instantaneous values of inductance [3].

The torque produced by SynchRM is purely reluctant. One of the main problems with this kind of machine is the power density and the power factor that are not very high, but new studies to increase the saliency rate of the machine [4]-[7] were developed to improve them making the SyncRM a real competitor to the asynchronous machine. Another advantage of the SyncRM is the absence of rare earth materials, which makes it an alternative to usual permanent magnet synchronous motors. The studied motor is shown in Fig. 1.

The SynchRM stator is similar to an asynchronous stator. Inside the rotor, flux barriers limit the magnetic flux in Q-axis direction. D-axis flux passes freely through iron parts between flux barriers (ribs). At extremities of flux barriers there are little iron bridges in place for mechanical issues. In an electromagnetically point of view these bridges are a problem, but they are narrow and their high saturation limit the flux passage.

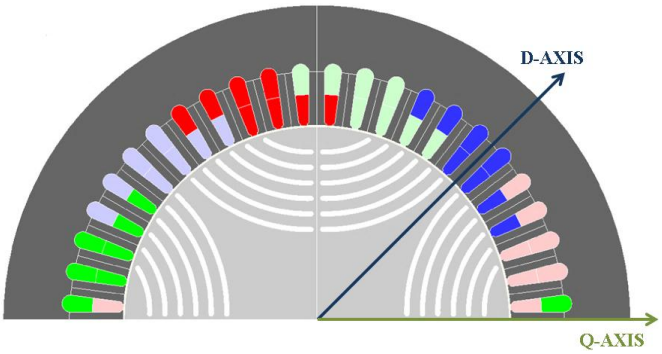

Fig. 1. SynchRM with flux barriers.

A method to build the MEC model of the SynchRM is proposed in this paper. In the first two parts the MEC of the stator and the rotor are presented and explained. The third part addresses the air-gap model and the rotor displacement. The fourth part is focused on coupling the MEC model with the electric circuit. The fifth part shows the results of the model. Finally, the last part makes a conclusion of the developed method, and sets the perspective for future works.

II. STATOR MODEL

The model of the machine is built in three steps, first the stator with validation after the rotor with validation and finally the air gap. Owing to symmetry, only one half of the machine was represented in our MEC model. Finite Element simulations (Flux2D software [17]) are used to build and validate the model.

For the stator study the rotor is considered homogeneous, isotropic and highly permeable (μr=10000) in order to decouple its effects. The stator material is a non-linear model

of the M400-50A iron steel. The studied geometry is shown in Fig. 2

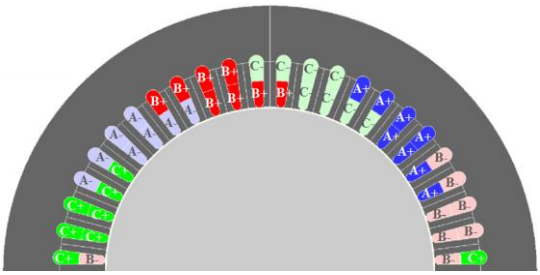

Fig. 2. Stator of the SynchRM

The three phases of the stator are fed by a three-phase current system (max value Ip). Magnetostatic simulations were made with several Ip and phase values.

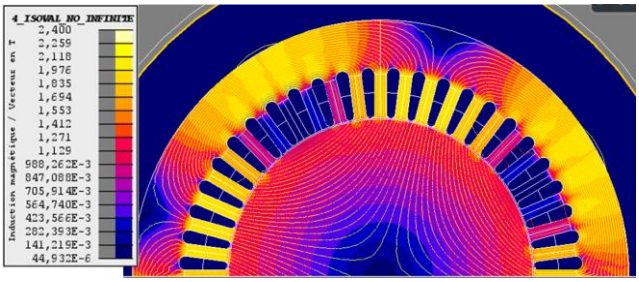

Fig. 3. Isoflux plot in the stator/Flux density with peak current value 65A.

With the Fig. 3 it is possible to analyze the flux paths, flux density and slots flux leakages. The levels of flux density are higher (2.4 T) in the teeth and on the top of the slots (this level of flux density is not reached in normal conditions of work). So these regions must be well discretized to make a correct MEC model. Fig. 4 shows the discretization of one tooth and also how the yoke is modeled. The lines inside the elements represent the model direction of the flux.

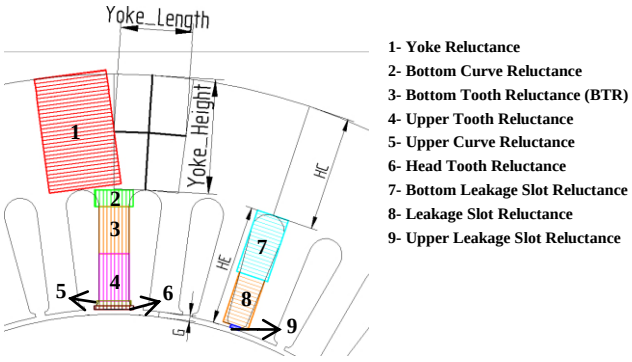

Fig. 4. Tooth and slot leakage model.

The formulation of one element as reluctance is defined by:

$$\Re = \frac{l}{\mu \cdot S} \tag{1}$$

where l is the length of the element, S the surface and μ is the permeability defined by the material and the flux density.

For example the yoke reluctance (rep1) is defined by:

$$Yoke\_length = \frac{\left(\left(\frac{HC}{2} + HE + Rotor\_Radius + G\right) \cdot \frac{\pi}{2}\right)}{48} \tag{2}$$

$$Yoke\_Surface = HC \cdot LM \tag{3}$$

where HC, HE and G are defined on Fig. 4, and LM is the length of the motor.

All the other elements are defined in the same way. The air gap will not be discussed now. At this step, air gap is simply modeled by an identified reluctance between each tooth and the rotor. The stator teeth are split in two parts to make possible the introduction of the slot leakage flux. The leakage reluctances are the elements 7, 8 and 9 in the Fig. 4.

With more reluctance elements the model becomes closer to the reality. But there is a compromise between number of elements and computation time.

In order to validate the stator model, many comparisons of the two methods (FEM and MEC) were made. For illustration the angular evolution of two tooth fluxes are shown in Fig. 5.

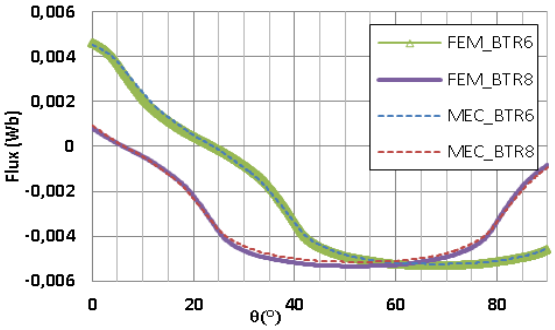

Fig. 5. Teeth flux evolution of the stator model with peak current value 65A.

The maximum difference between the models is about 4.5%. This dereference is considered as satisfactory and the model of the stator is considered as validate.

III. ROTOR MODEL

The SynchRM has a very complex structure of rotor which makes the evaluation of flux paths and flux density more complex. So the work is going to be made in two different parts. Firstly, the motor is going to be excited only in Q-axis. Then in a second stage the D-axis is going to be excited.

A. Q-axis excitation

Fig. 6 shows how the flux flows in the rotor with a Q-axis excitation.

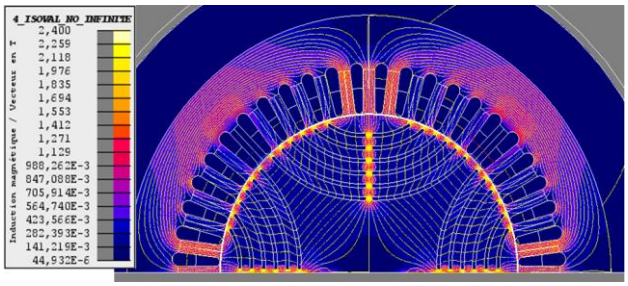

Fig. 6. Isoflux/Flux density purely Q-axis excitation (65A peak value).

The analysis of Fig. 6 shows that the main flux path is in the bridges between flux barriers. There are also the flux paths that pass through flux barriers. They are considered as leakage fluxes since the flux barriers are made by air.

When analyzing the flux density in the rotor it is very clear that the saturated areas are the bridges at the extremities of flux barriers. The bridges are going to be high saturated since they have a very narrow path to pass the flux. Fig. 7 shows how the external bridges and the flux barriers were modeled.

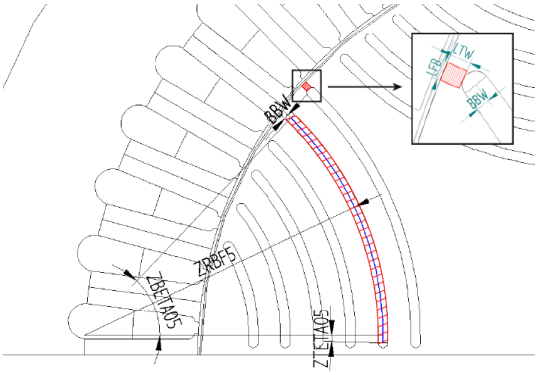

Fig. 7. Flux Barriers Modeling and external bridges model

The external bridge is modeled as it follows:

$$External\_Bridges\_Length = LFB = 1.35 * BBW \quad (4)$$

$$External\_Bridges\_Surface = LTW \cdot LM \quad (5)$$

The internal and external bridges are the most saturated elements of the model, so it is crucial to well model these elements. To find the length value (1.35 BBW) several tests were necessary to reduce the error to a minimal level. The internal bridges are not shown in this paper but they are modeled exactly the same way.

B. D-axis excitation

Fig. 8 shows the flux density and the flux lines in the motor for the case of a D-axis excitation.

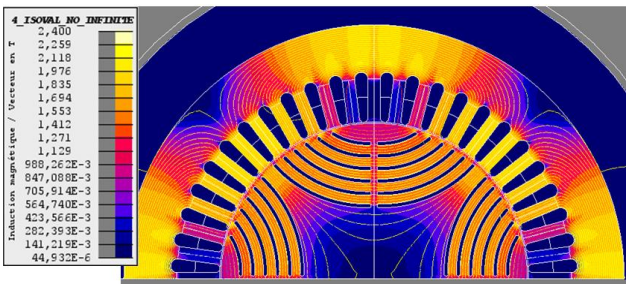

Fig. 8. Isoflux/Induction purely D-axis excitation (65A peak value).

With this excitation the main flux paths are located between the flux barriers (ribs), instead of flowing through the flux barriers. The flux density in these regions is homogeneous and allows a model with only two elements per rib.

Another important observation is that in this case the stator is more saturated than the rotor. This means that an error made in the stator model will directly reflect in the rotor model.

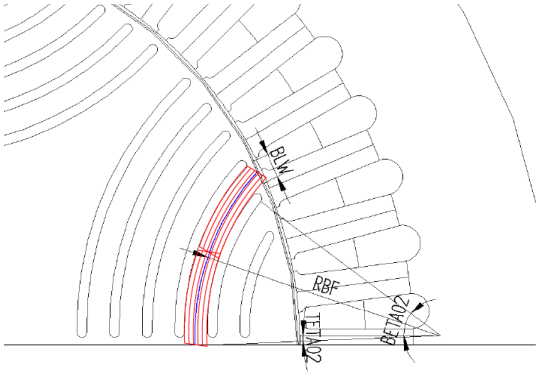

Fig. 9. Rib model.

Fig. 9 shows how the ribs are modeled. The rib is split in two parts to introduce the leakage of the flux barrier when the two axes "D" and "Q" are excited simultaneously. The validation can also be made by a comparison between the fluxes in certain regions of the rotor when Iq varies. In the Fig. 10 two fluxes are compared with the FEM simulation, the concerned elements are the most saturated part in the rotor, the bridges near the air gap (external bridges).

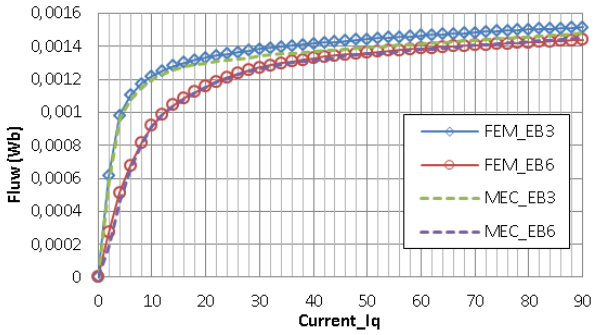

Fig. 10. Evolution of two external bridge fluxes with Q excitation current.

Comparing the results of the two models the difference between them is around 2.5%, so the model is considered valid.

Finally the half of the model of the rotor and the stator is shown in Fig. 11. The air-gap is going to be discussed further.

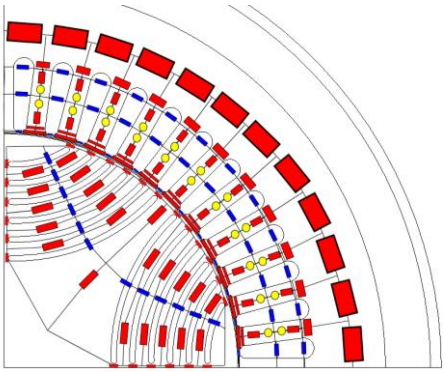

Fig. 11. Stator and Rotor MEC model.

The model of half motor is represented by 414 elements in total, not taking into account air gap elements.

IV. Rotor Movement

A. Air-gap Definition

The air-gap reluctance can be determined by the flux that flows in the air-gap. Many papers tried to determine the flux density or the flux flow in the air-gap [8]-[14]. But they are very complicated to implement in a MEC model, and they may increase the model calculation time.

The chosen method is to cut the rotor surface into zones and then consider a reluctance between each zone and each tooth. Each reluctance varies with the rotor position. To evaluate them a FEM analysis was made.

Two punctual singular MMF sources (1A) are put in one tooth as can be seen in Fig. 12 (S1, S2). The stator and rotor material is modeled with high permeability (μ_r=10000), the rotor has no flux barriers.

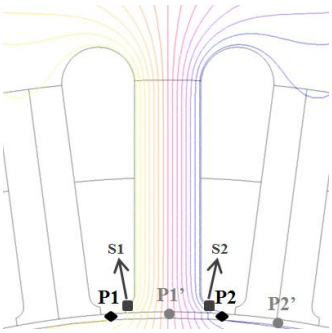

Fig. 12. EF simulation for air gap definition.

The goal of this simulation is to evaluate the flux that flows from the fed tooth to the rotor. The points P1 and P2 determine a certain zone of the rotor. The points P1' and P2' represents the same zone after a given rotor displacement θ.

The value of the air gap reluctance of the zone determined by P1 and P2, is given by:

$$\Re = \frac{N \cdot I}{\phi} \Rightarrow \frac{1}{\phi_{P1}(\theta) - \phi_{P2}(\theta)} \tag{6}$$

From (7) it can be seen that the flux varies with the rotor position (θ). So it is absolutely necessary to know the evolution of the flux with the rotor position.

So Fig. 13 is plotted by the FEM analysis. It shows how the flux changes with the rotor position.

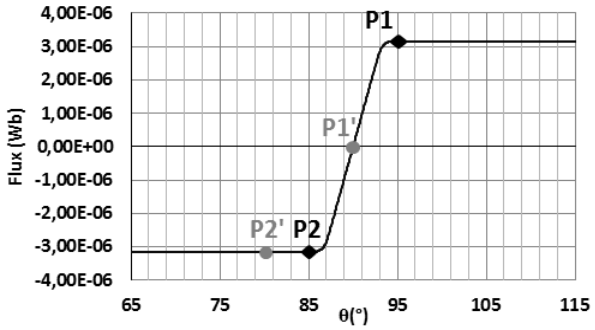

Fig. 13. Flux in the air-gap.

A Fourier series F(θ) is obtained from this curve (Fig. 13) and used as the function to determine the reluctance value:

$$\Re = \frac{1}{F(P1+\theta) - F(P2+\theta)} \tag{7}$$

where θ is the rotor position, P1 and P2 are the positions of the points defining a certain zone when θ=0.

The problem of this method is that it is not possible to change the parameters of the motor model, since the Fourier series are imposed by the geometry of the machine. Currently a parametrized analytical model is being developed in order to replace the Fourier series. This work will be published later.

B. Sources Displacement

In [15] the model connects all the stator teeth to all rotor zones. However this technique has a limitation due to the high number of air-gap reluctances needed for the modeling.

Perez shows in [16] another technique in which the MMF is defined by only the first harmonic, which makes the sources displacement easier, since the change in the source value is made directly in the angle of the harmonic.

Based on these ideas a mixed model is created. The first step is to discretize the rotor in some zones; in this case, bridges fix them. Each zone has an interaction with some of the stator teeth represented by an air reluctance which value changes with position rotor position.

In the Fig. 14a the example shows that the zone 1 of the rotor has interactions only with the teeth 1, 2 and 3 of the stator. All other teeth interactions are neglected. Once θ is higher than one stator tooth pitch the connection changes to the teeth 2, 3 and 4. Instead of completely changing the MEC the method shown in Fig. 14b is adopted, in it once θ is superior to stator tooth pitch the sources of MMF will change places.

To sum up, between 0 < θ < (tooth pitch) the reluctance are depending of rotor position θ. For θ higher than tooth pitch the sources change places to avoid a new MEC, which reduces

computational time and does not change the accuracy of the model.

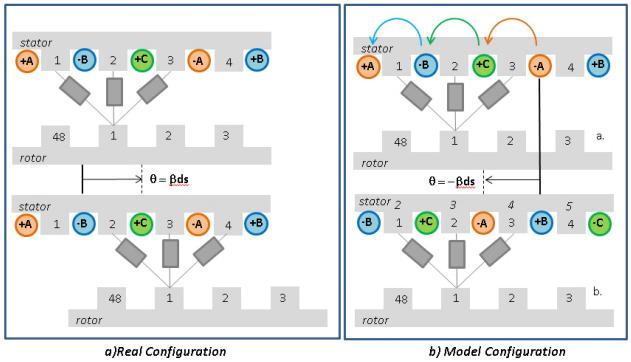

Fig. 14. Source displacement.

In Fig. 15 it is shown some of the MMF definitions for the low layer winding before and after the source rotation.

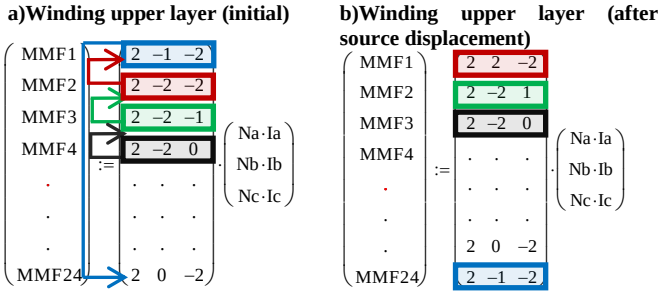

Fig. 15. Source rotation.

V. Circuit Coupling

The model is controlled by MMF sources, so phase currents are inputs of model instead of voltage. An extension of model is necessary to make possible the connection to a circuit simulator. Based on (8) it can be deduced a way to calculate the current using the outputs of the model and its derivatives.

$$V = \frac{d\lambda}{dt} + R \cdot i \Rightarrow \frac{d\lambda}{di} \cdot \frac{di}{dt} + \frac{d\lambda}{d\theta} \cdot \frac{d\theta}{dt} + R \cdot i \qquad (8)$$

Equations (9), (10) and (11) are expansions of (8) for the three phases of the motor.

$$Va = \frac{d\lambda a}{dia} \cdot \frac{dia}{dt} + \frac{d\lambda a}{dib} \cdot \frac{dib}{dt} + \frac{d\lambda a}{dic} \cdot \frac{dic}{dt} + \frac{d\lambda a}{d\theta} \cdot \omega + R \cdot ia \quad (9)$$

$$Vb = \frac{d\lambda b}{dia} \cdot \frac{dia}{dt} + \frac{d\lambda b}{dib} \cdot \frac{dib}{dt} + \frac{d\lambda b}{dic} \cdot \frac{dic}{dt} + \frac{d\lambda b}{d\theta} \cdot \omega + R \cdot ib \quad (10)$$

$$Vc = \frac{d\lambda c}{dia} \cdot \frac{dia}{dt} + \frac{d\lambda c}{dib} \cdot \frac{dib}{dt} + \frac{d\lambda c}{dic} \cdot \frac{dic}{dt} + \frac{d\lambda c}{d\theta} \cdot \omega + R \cdot ic \quad (11)$$

From (9), (10) and (11) it is possible to control the motor by voltage instead of current. These expressions of the phase voltages are used to couple our model with a circuit simulator (PSIM and Matlab/Simulink).

VI. Results

The MEC model has also the advantage of providing the Jacobean, so since the co-energy (w*) of the MEC model is already calculated, the electromagnetic torque is estimated directly from:

$$T_{em} = \frac{dw^*}{d\theta} \qquad (12)$$

The results from (12) are obtained directly from the Jacobean of the model.

Fig. 16 shows a comparison between the torque obtained by the FEM and MEC models with three phase currents.

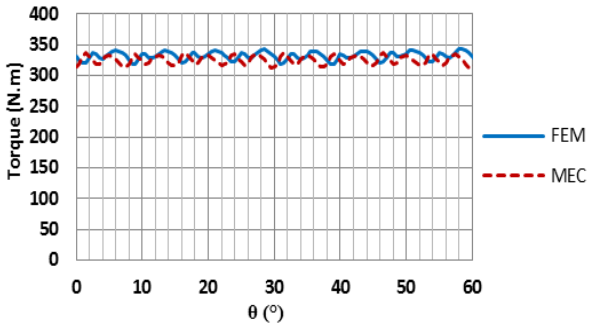

Fig. 16. Torque result for 3 phases current fed model (65A).

The max difference between the two methods is 6.5%. What is remarkable in this result is that the model has a phase difference of 1°, but both of them have the same torque ripple appearance. The difference in the average torque is 2,1%.

Fig. 17 shows the results when the windings of the models are suddenly connected to a three-phase voltage source synchronized with the rotation. (1000V, 25Hz, 1800rpm, R=1ohm).

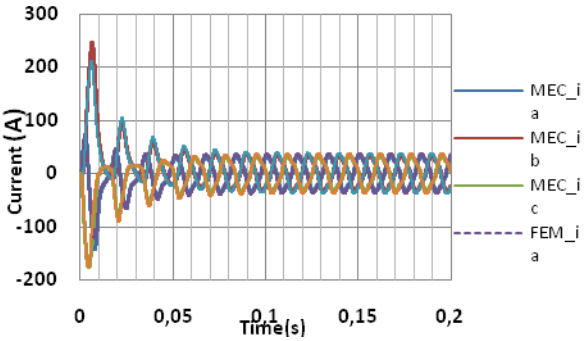

Fig. 17. Current result for voltage fed model.

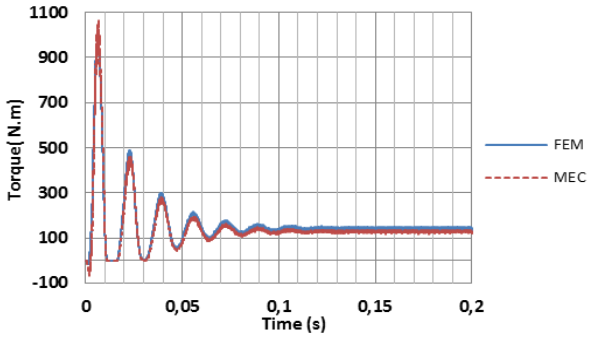

Fig. 18. Torque result for voltage fed model.

The torque difference (Fig. 18) in steady state is 9.9%, which is higher than before due to the addition of the error of

the current calculation (which is not present when the current is imposed). It also can be seen that the model response in transient region is quite accurate.

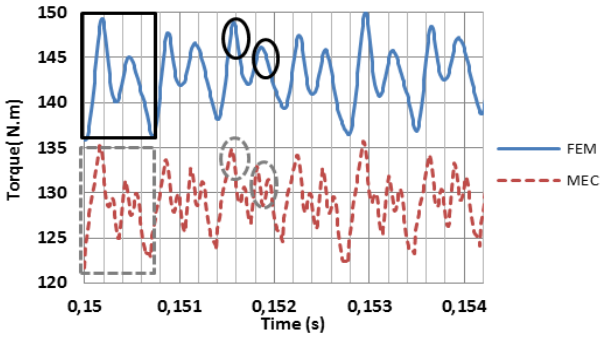

Fig. 19. Torque result for voltage fed model zoom

Fig. 19 shows a zoom in the torque results from Fig. 18. The rectangles show the torque ripple caused by the slots (tooth period). Two consecutive periods are not the same because of windings distribution. The circles show the ripple due to the interaction between rotor zones and teeth.

The other torque variations which appear only in the MEC model are characteristics of the model, but it can be seen that the torque ripple is well represented even with such problems.

VII. Conclusion

This paper has shown an effective technique to create accurate dynamic (multistatic) MEC model. The results are very satisfactory and the torque ripple is well represented. Many difficulties were overcome, including the modeling of the air gap, the movement of the motor and the coupling with the electric circuit.

A new model of the air gap is currently being developed and will be presented in a future paper.

The model has yet the advantage to be coupled directly with an electric circuit simulator (PSIM, Matlab/Simulink...) to test motor control.

It is also important to add that the development of model in CADES software [18] has the advantage of giving the Jacobean, which is another advantage when compared with the FEM model. The Jacobean allows access to the instantaneous inductance, and also is very important to the motor optimization afterwards [2].

The calculation time for our MEC model is significantly reduced(four times) when compared with the FEM model. (you have additional outputs of the modeling in addition to magnetic information B, L , flux … your have) the time comparison includes time of post processing at FEM tool? At your tool ?

acknowledgment

The authors thank Tiago Staudt [ref] for his effective assistance to the development of the model.

References

[1] V. Ostovic, “Magnetic Circuits,” in Dynamics of Saturated Electric Machines , 1th ed. New York, Springer-Verlag, 1989, pp. 29–54.

[2] B. Delinchant, D. Duret, L. Estrabaut, L. Gerbaud, H. Huu, B. Du Peloux, H. Rakotoarison, F. Verdière, F. Wurtz, An optimizer using the software component paradigm for the optimization of engineering systems, COMPEL: The International Journal for Computation and Mathematics in Electrical and Electronic Engineering, v. 26, n. 2, p. 368-379, 2007.

[3] B. duPeloux , L. Gerbaud , F. Wurtz , V. Leconte and F. Dorschner "Automatic generation of sizing static models based on reluctance networksfor the optimization of electromagnetic devices", IEEE Trans. Magn., vol. 42, pp.715 -718 2006

[4] M. J. Kamper, “Design Optimisation of Cageless Flux Barrier Rotor Reluctance Synchronous Machine,” Ph.D. dissertation,Univ. Of Stellebosch, Stellebosch, South Africa, 1996.

[5] Tsaarady Raminosoa. “Optimisation des Performances des Machines Synchro-Reluctantes par Reseaux de Permeances”. Micro and nanotechnologies/Microelectronics. Institut National Polytechnique de Lorraine - INPL, 2006. French.<tel-0126662>.

[6] J. G. Wright, “Design of a Synchronous Machine for Traction Motor Applications Using The Finite Element Method,” M.S. thesis, Univ. of Witwatersrand, Johannesburg, South Africa, 2010.

[7] R. R. Moghaddam “Synchronous Reluctance Machine(SynRM) Design” M.S. thesis, Royal Institute of Technology, Department of Electrical Engineering Electrical Machines and Power electronics, Stockholm 2007.

[8] E. Ilhan, M. F. Kremers, , E. T. Motoasca,J. J. H. Paulides and E. A. Lomonova, “Spatial Discretization Methods for Air Gap Permeance Calculations in Double Salient Traction Motors,” IEEE Trans. on Industry Apli., vol. 48, no. 6, pp. 2165-2172, Nov/Dec., 2012.

[9] Z. Q. Zhu, D. Howe, E. Bolte, B. Ackermann, “Instantaneous Magnetic Field Distribution in Brushless Permanent Magnet dc Motors, Part I: Open-Circuit Field,” IEEE Trans. Magn., vol. 29, no. 1, pp. 124-135, Jan., 1993.

[10] Z. Q. Zhu, D. Howe, “Instantaneous Magnetic Field Distribution in Brushless Permanent Magnet dc Motors, Part II: Armature-Reaction Field,” IEEE Trans. Magn., vol. 29, no. 1, pp. 136-142, Jan., 1993.

[11] Z.Q. Zhu, D. Howe, “Instantaneous Magnetic Field Distribution in Brushless Permanent Magnet dc Motors, Part III: Effect of Stator Slotting,” IEEE Trans. Magn., vol. 29, no. 1, pp. 143-151, Jan., 1993.

[12] Z. Q. Zhu, D. Howe, C. C. Chan, “Improved Analytical Model for Predicting the Magnetic Field Distribution in Brushless permanent Magnet Machines,” IEEE Trans. Magn., vol. 38, no. 1, pp. 229-238, Jan., 2002.

[13] D. Zarko, T. A. Lipo, D. Ban, “Analytical Calculation of Magnetic Field Distribution in the Slotted Air Gap of a Surface PM Motor Using Complex Relative Air Gap Permeance,” IEEE Trans. Magn., vol. 42, no. 7, pp. 1828-1837, Jul., 2006.

[14] K. F. Rasmussen, J. H. Davies, T. J. E. Miller M.I. McGlip, M. Olaru, “Analytical and Numeriacl Computation of Air-Gap Magnetic Fields in Brushless Motors with Surface Permanent Magntes,” IEEE Trans. on Industry Apli., vol. 36, no. 6, pp. 1547-1554, Nov./Dec., 2000.

[15] H. Dogan, L. Garbuio, H. Nguyen-Xuan, B. Delinchant, A. Foggia, F. Wurtz “Multistatic Reluctance Network Modeling for the Design of Permanent-Magnet Synchronous Machines,” IEEE Trans. Magn., vol. 49, no. 5, pp. 2347-2350, May, 2013.

[16] Sylvain Perez. Contribution au Dimensionnement Optimal d'Alternateur à Grifes Sans Aimant- Apport des alliages FeCo. Engineering Sciences. Universite de Grenoble, 2013. French.<NNT: 2013GRENT094>.<tel-00990653v2>

[17] FLUX, CEDRAT, http://www.cedrat.com

[18] CADES, http://www.vesta-system.com

References :

[19] - IEEE TRANSACTIONS ON MAGNETICS, VOL. 50, NO. 5, MAY 2014 7026909 A Seminumerical Finite-Element Postprocessing Torque Ripple Analysis Technique for Synchronous Electric Machines Utilizing the Air-Gap Maxwell Stress Tensor Christopher M. Spargo, Barrie C. Mecrow, and James D. Widmer School of Electrical and Electronic Engineering, University of Newcastle Upon Tyne, Newcastle Upon Tyne NE1 7RU, U.K.

3406 IEEE TRANSACTIONS ON MAGNETICS, VOL. 43, NO. 8, AUGUST 2007 Comparison Between Finite-Element Analysis and Winding Function Theory for Inductances and Torque Calculation of a Synchronous Reluctance Machine Thierry Lubin, Tahar Hamiti, Hubert Razik, and Abderrezak Rezzoug Groupe de Recherche en Electrotechnique et Electronique de Nancy, GREEN-CNRS UMR-7037, Université Henri Poincaré, BP 239, 54506 Vandoeuvre-lès-Nancy Cedex, France

[20] Iron and Magnet Losses and Torque Calculation of Interior Permanent Magnet Synchronous Machines Using Magnetic Equivalent Circuit Abdul Rehman Tariq, Carlos E. Nino-Baron, and Elias G. Strangas

Department of Electrical and Computer Engineering, Michigan State University, East Lansing MI 48824 USA